Modeling Molecular Mechanisms of Binding of the Anaphylatoxin C5a to the C5a Receptor†

Gregory V. Nikiforovich,*,‡ Garland R. Marshall,‡ and Thomas J. Baranski§

Center for Computational Biology, Department of Biochemistry and Molecular Biophysics, and Departments of Medicine and of Molecular Biology and Pharmacology, Washington University Medical School, St. Louis, Missouri 63110

Received November 23, 2007; Revised Manuscript Received January 11, 2008

ABSTRACT: This study presents the 3D model of the complex between the anaphylatoxin C5a and its specific receptor, C5aR. This is the first 3D model of a G-protein-coupled receptor (GPCR) complex with a peptide ligand deduced by a molecular modeling procedure analyzing various conformational possibilities of the extracellular loops and the N-terminal segment of the GPCR. The modeling results indicated two very different ways of interacting between C5a and C5aR at the two interaction sites suggested earlier based on the data of site-directed mutagenesis. Specifically, C5a and C5aR can be involved in "mutual-induced fit", where the interface between the molecules is determined by both the receptor and the ligand. The rigid core of the C5a ligand selects the proper conformations of the highly flexible N-terminal segment of C5aR (the first interaction site). At the same time, the binding conformation of the flexible C-terminal fragment of C5a is selected by well-defined interactions with the TM region of the C5aR receptor (the second interaction site). The proposed 3D model of C5a/C5aR complex was built without direct use of structural constraints derived from site-directed mutagenesis reserving those data for validation of the model. The available data of site-directed mutagenesis of C5a and C5aR were successfully rationalized with the help of the model. Also, the modeling results predicted that the full-length C5a and C5a-des74 metabolite would have different binding modes with C5aR. Modeling approaches employed in this study are readily applicable for studies of molecular mechanisms of binding of other polypeptide ligands to their specific GPCRs.

The anaphylatoxin C5a is an important molecular component participating in activation of a complement system in response to infection [see, for example, the brief review of physiological activities of C5a (*1*)]. It is a potent chemotactic factor for neutrophils, eosinophils, basophils, macrophages, and microglial cells. Also, C5a causes demargination and infiltration of leukocytes, release of proteolytic enzymes, superoxide production, capillary leakage, and smooth muscle contraction. The peptide chain of C5a consists of 74 amino acids; in solution, the first 62 residues are well-organized into a disulfide-linked core, and the C-terminal tail remains unstructured (*2, 3*). Biological activities of C5a are specifically mediated through its receptor C5aR,[1] which is widely expressed in inflammatory cells; accordingly, agents that act on C5aR hold great potential as therapeutics.

The 350 amino acid–protein, human C5aR, belongs to the wide group of G-protein-coupled receptors (GPCRs), the largest protein family in humans. GPCRs are embedded in the cell membrane and include seven helical transmembrane stretches (TM helices), the N- and C-terminal fragments (the extracellular N-terminal fragment is often glycosylated), and both extra- and intracellular loops (EC and IC loops) connecting the TM helices. The amino acid sequence of human C5aR is homologous to the sequence of rhodopsin, until very recently the only GPCR for which a three-dimensional (3D) structure of the dark-adapted state was available in high resolution (*4–8*). [Two X-ray structures of human β2-adrenergic receptor showed the 3D structure of the TM region of this receptor remarkably close to that of rhodopsin (*9, 10*).] C5aR also resembles rhodopsin by the size of its EC and IC loops. One may expect, therefore, that elucidation of the structural basis of interaction between C5a and C5aR would not only facilitate the rational design of potential regulators of inflammation but also be relevant to the more general problem of activation of GPCRs by polypeptide ligands such as chemokines, chemotactic factors, peptide hormones, and others. This has great clinical significance given that GPCRs represent about 50% of targets for drugs currently in clinical use (*11*).

Currently, there is no detailed 3D model of the complex of C5a with C5aR. The available data of site-directed mutagenesis support a "two-site" model of interaction between C5a and C5aR (*12–14*). A C5aR mutant lacking the first 22 N-terminal residues did not bind C5a, but the truncated receptor could be effectively activated by an analogue of the C-terminal octapeptide of C5a (*14*), the

† This work was partly supported by NIH Grants GM 68460 (G.V.N. and G.R.M.), GM 71634 (G.V.N. and T.J.B.) and GM63720 (T.J.B.).

* To whom correspondence should be addressed. Tel: 314-362-1566. Fax: 314-362-0234. E-mail: gregory@ccb.wustl.edu.

‡ Center for Computational Biology, Department of Biochemistry and Molecular Biophysics.

§ Departments of Medicine and of Molecular Biology and Pharmacology.

[1] Abbreviations: 3D, three-dimensional; C5aR, C5a receptor; GPCR, G-protein-coupled receptor; TM; transmembrane helix; IC, intracellular loop; EC, extracellular loop; PDB, Protein Data Bank; NMR, nuclear magnetic resonance; SDSL, site-directed spin labeling.

10.1021/bi702321a CCC: $40.75
Published on Web 02/15/2008

smallest C5a fragment with reasonable binding affinity (*15*). It was suggested, therefore, that one site of binding is located in the N-terminal fragment of C5aR (the "first site") and that the C-terminal fragment of C5a binds another site in C5aR located in the TM region (the "second site").

Specific residue–residue interactions between C5a and C5aR were assigned based almost exclusively on the data of site-directed mutagenesis of C5a and C5aR. Modifications of the C-terminal residues of C5a, such as His67, Lys68, Leu72, and, especially, Arg74, lead to a significant decrease of binding toward C5aR (*12*) (the C5a residues are denoted for convenience by three-letter notation, while the C5aR residues are denoted by one-letter notation). The importance of Arg74 was confirmed in subsequent studies (*16*); however, the possible involvement of Arg40 in contact with C5aR suggested earlier (*12*) was not confirmed (*16*). The same paper reported more than a 50-fold decrease in biological activity of the C5a analogues due to the double replacement (Lys19Ala, Lys20Ala) (*16*). Another study found a 3–7-fold decrease in binding affinity of the C5a analogues with single replacement of Lys19, Lys20, or Arg40 by alanine; it also pointed out the importance of mutations His15Ala (10-fold decrease in binding), Val18Asp (712-fold decrease), Asn37Asp (84-fold), Arg46Ala (17-fold), and, again, Arg74Ala (600-fold) (*17*). Multiple mutations lead to even greater decreases in affinity, such as a 296-fold decrease when both His15 and Arg46 were replaced by alanines, 500-fold for the triple mutation (His15Ala, Leu43Ala, Lys49Ala), and 4000-fold for the multiple mutation (His15Ala, Leu43Ala, Lys49Ala, Glu53Ala, Arg46Ala) (*17*).

In studies focused on the N terminus of C5aR, simultaneous alanine substitutions for aspartic acid residues D15, D16, D18, and D21 in the N-terminal fragment (the suggested first binding site) led to a 40-fold decrease of affinity for C5a, and the additional mutation D10A caused an additional 90-fold decrease in binding (*14*). At the same time, single replacements of D10 and D27 by asparagines or the double mutation (D21N, D27N) did not affect affinity to C5a, but receptors with simultaneous replacements of D10, D15, and D16 or D10, D15, D16, D21, and D27 by asparagines did not bind C5a (*18*). However, the NMR data on the interaction of C5a with the N-terminal segment of C5aR 1–34 in water revealed that only D21 and D27 were perturbed by C5a binding (*19*). Additional studies demonstrated that two tyrosines in the N terminus, Y11 and Y14, are sulfated in a posttranslational step and that sulfation is critical for efficient binding of C5a (*20*). Recent work using random saturation mutagenesis of the N-terminal fragment of C5aR in yeast demonstrated that no single residues in the N terminus are essential for ligand activation of the receptor (*21*). Furthermore, many of the mutated C5a receptors that demonstrated activity also contained cysteine substitutions within the fragment 24–30 of C5aR, suggesting that the unpaired cysteine Cys27 in the C5a ligand might contact this region (*21*). Also, the very recent development employing the novel technique of disulfide trapping by random mutagenesis in yeast showed the possibility of contacts between specific regions of the N-terminal fragment of C5aR and specific residues of C5a (*22*).

Mutational studies of the second binding site in C5aR focused on residues E199 and R206 in the transmembrane helix (TM) TM5 and on D282 in TM7. The results obtained and their interpretation varied from study to study. For instance, binding of C5a to the C5aR mutant E199R was decreased by about 7-fold as compared to the binding to the wild-type C5aR (WT), but the C5a analogue [Lys68Glu] displayed stronger binding to E199R receptors (*23*). These results imply that the two residues, E199 and Lys68, might participate in a salt bridge facilitating binding of C5a to C5aR, although it was suggested that this interaction may not be essential in receptor activation (*23*). However, in other studies, C5a bound equally well to both the WT and the E199Q mutant (*24*) and elicited similar biological responses through either WT or E199K receptors (*25*). Elimination of the side chain of R206 in the R206A mutant led to the complete loss or approximately 7-fold reduction of C5a binding (*26* and *27*, respectively), but another study reported approximately the same binding affinity of C5a for WT and R206A (*28*). More recent work found a 3-fold decrease in the binding affinity of C5a toward R206A (*29*). Regarding D282, although C5a was found not to bind to the D282A mutant (*26*), a different study showed the same mutation caused only a 2-fold decrease in activation by C5a as compared to WT (*25*) and the same binding affinity as that for WT in another study (*27*). Reversing the charge in a D282R mutant decreased C5a binding affinity 4-fold (*27*), but the mutant showed about 60-fold decrease in biological response to C5a (*25*). In the EC2 loop of C5aR, R175A and R175D mutations both showed significant decrease in biological response to C5a (*25*) and in C5a binding (*29*). It is also noteworthy that several mutations in the EC1 loop of C5aR (positions 103 and 105) did not change the binding affinity to C5a (*30*).

Generally, it would be quite difficult to generate a 3D model of the C5a−C5aR complex employing only the experimental data briefly summarized above. Several attempts to build a model were made with the use of the experimental 3D structure of dark-adapted rhodopsin as a prototype for the 3D structure of C5aR, as well as the NMR-deduced structures of C5a (*21*) or of the oligopeptide C5a agonists/antagonists (*29, 31*). While the 3D structures of the TM regions of rhodopsin and C5aR are likely to be similar based on high homology between the two regions, the 3D structures of the extracellular parts of rhodopsin and C5aR directly involved in binding of C5a may be very different. This is not surprising since the extracellular domains in different GPCRs need to have different 3D structures for molecular recognition of specific ligands that vary in size and shape. That was clearly demonstrated very recently with the novel X-ray structure of human β2-adrenergic receptor, where conformation of the EC2 loop was dramatically different from that observed in rhodopsin (*10*).

Nontransmembrane segments of a GPCR possess much higher conformational flexibility as compared to the TM bundle itself [see, for example, multiple conformations of the IC loops of rhodopsin found in different X-ray structures (*4–8*); also, the N-terminal extracellular fragment, the EC loops, and, partly, the IC3 loop and the C-terminal segment were disordered in one of the recent X-ray structure of the β2 adrenergic receptor (*9*)]. In this situation, experimental methods usually produce either the averaged model of the fluctuating structure (such as in the NMR studies of highly flexible linear peptides) or single snapshots of the structure in a crystalline lattice (such as those obtained by

X-ray spectroscopy). In contrast, molecular modeling approaches can account for high conformational flexibility of the extracellular parts of GPCRs by sampling various low-energy conformations of the EC loops and the N-terminal fragments as well as various possible orientations of the ligands relative to the receptor. This modeling approach was successfully applied in our previous studies for determining possible conformations of the EC and IC loops in rhodopsin (*32*), the IC loops in C5aR (*33*), and orientations of the C-terminal fragment of the α-subunit of transducin within the cavity formed by the IC loops of photoactivated rhodopsin (*34*). This approach was used in the present study to generate a model(s) of the complex between C5a and C5aR accounting for the flexibility of the EC loops and the N-terminal fragment of C5aR to rationalize available and future mutagenesis data. Our modeling of the docking of C5a to its receptor did not employ specific experimental constraints derived from site-directed mutagenesis for determining the system of residue–residue interactions between C5a and C5aR. It allowed use of the experimental data from site-directed mutations to be reserved for validation of the proposed 3D model of the C5a/C5aR complex.

MATERIALS AND METHODS

Most essential modeling procedures employed in this study and their general outcome are briefly described below (see also Table S1 in Supporting Information). Additional technical details of computational procedures also are presented in the Supporting Information.

Force Field. Energy calculations employed the ECEPP/2 force field (*35, 36*) with rigid valence geometry and planar *trans*-peptide groups (except those for prolines, where the ω angles were varied). Energy calculations were routinely performed with one of the two different values of the macroscopic dielectric constant, either $\epsilon = 2$ (the standard value for ECEPP corresponding to protein environment) or $\epsilon = 80$ (a value corresponding to water). In our view, introducing distant-dependent values for ϵ, as well as possible accounting for nonexplicit water and/or lipid environment, would not improve energy estimations significantly; at the same time, introducing explicit water molecules in the system would require excessive computational resources (see also the Results section).

Build-up Procedures for C5a 59–74 and C5aR 8–41. A search for low-energy conformations of the C-terminal fragment 59–74 of C5a and the N-terminal fragment 8–41 of C5aR was performed using the well-established build-up procedure of stepwise elongation of the corresponding peptide chains (*37*). For C5a 59–74, energy calculations yielded 157 nonredundant low-energy backbone conformers (those with the energy cutoff $\Delta E = E - E_{min} < 10$ kcal/mol); the backbone conformation was considered unique (nonredundant) if one or more of the backbone torsion angles differed by more than 40° from the corresponding angle of any other low-energy conformation. The low-energy conformations were then clustered into 30 clusters defined by the rms value of 2 Å (C^{α} atoms only). For C5aR 8–41, elongation from 33 nonredundant low-energy conformers found for C5aR 8–24 was proceeded to 8–28 (140 nonredundant low-energy conformers found) to 8–31 (75) to 8–34 (99) to 8–41 (185). We did not elongate the N-terminal segment beyond fragment 8–41 to fragment 1–41 because of difficulties in modeling a carboxyhydrate moiety in the N-glycosylated site located at residue N5 in human C5aR (*38*) and because the first seven residues of C5aR can be replaced without any loss in C5a binding (*18*).

Building of TM Region of C5aR. The procedure for building the TM bundle of the C5aR was essentially the same as described previously (*33*). First, transmembrane helical fragments were located in the sequence of the human C5aR by sequence homology to rhodopsin helices found by the CLUSTAL W procedure (http://ca.expasy.org/tools). The TM helices were thus determined as follows: TM1, I38-V50-A63 (the first, middle, and last residue, respectively); TM2, N71-L84-Q98; TM3, A107-A122-V138; TM4, A150-W161-F172; TM5, E199-F211-F224; TM6, R236-F251-F267; and TM7, L281-Y290-Y300. The helical fragments were then assembled in a TM helical bundle following the procedure of "enhanced homology modeling" (*39*) consisting of (i) determining conformations of individual helices by independent energy minimization involving all dihedral angles starting from the values corresponding to the rhodopsin TM helices; (ii) superimposing the obtained conformations over the X-ray structure of Rh according to sequence homology; and (iii) assembling helices by finding the energetically best arrangement of the individual helices, in which dihedral angles of the backbone are "frozen" in the values obtained earlier. In fact, assembling consisted of minimization of the sum of all intra- and interhelical interatomic energies (with $\epsilon = 2$) in the multidimensional space of parameters that included the $6 \times 7 = 42$ "global" parameters (those related to movements of individual helices as rigid bodies, namely, translations along the coordinate axes *X*, *Y*, *Z* and rotations around these axes T_x, T_y, and T_z) and the "local" parameters [the dihedral angles of the side chains for all helices; the starting values of the angles were those repacked prior to energy minimization by an algorithm described earlier (*40*)].

The coordinate system for the global parameters was selected as follows: the long axial *X* coordinate axis for each TM helix (TM1−TM7) has been directed from the first to the last C^{α} atom; the *Y*-axis was perpendicular to *X* and went through the C^{α} atom of the "middle" residue of each helix; and the *Z*-axis was built perpendicular to *X* and *Y* to maintain the right-handed coordinate system. The starting point for global parameters was that of the X-ray structure of the dark-adapted rhodopsin [the Protein Data Bank (PDB) entry 1F88].

Restoring the EC Loops. The procedure for restoring possible low-energy conformations of the EC loops on the template of the TM region of C5aR was essentially the same as performed earlier for the EC and IC loops of rhodopsin (*32*) and for the IC loops of C5aR (*33*). Specifically, geometrical sampling of the individual loops was performed by stepwise elongation of all loops, from the smallest loop to the largest, that is, from EC1 (Q98-A107) to EC3 (F267-L281) to EC2 (F172-E199). As soon as the resulting structures of the smaller loops were selected, the loop structure closest to the average spatial positions of the C^{α} atoms was included in the template, providing additional geometrical limitations for the larger loops. Energy calculations yielded 23 low-energy structures (those with the energy cutoff $\Delta E = E - E_{min} \leq 10$ kcal/mol) that formed three clusters of similar structures (defined by an rms value ≤2

Å, C^{α} atoms only) for EC1; 44 structures within $\Delta E \leq 15$ kcal/mol falling into 22 different clusters for EC3; and 881 structures within $\Delta E \leq 50$ kcal/mol falling into 24 different clusters (the rms cutoff ≤3 Å) for EC2. The lowest-energy conformers in each cluster were selected as representatives for further consideration in the extracellular "package" comprising all combinations of conformations for EC1 + EC2 + EC3 (1584 combinations). Then, for the set of combinations of representatives, energy calculations were performed with the same limitations as those described earlier (*32*); the TM helical stems included in the "package" were kept in the same positions as in the TM region by the rigid linkers consisting of the dummy atomic centers. The known C109−C188 disulfide bridge was modeled by the corresponding system of parabolic potentials. Finally, 310 low-energy structures for the EC1 + EC2 + EC3 package ($\Delta E \leq 50$ kcal/mol) were selected. They formed 29 clusters of similar structures (the rms cutoff ≤3 Å), and the lowest-energy conformation for each cluster was selected as its representative structure.

Assembling C5aR and Fragments of C5a. The "most open" conformation of the individual EC loops selected out of the 29 representative structures of the EC1 + EC2 + EC3 package as that providing the maximal distance between the "tips" of EC2 (C_{177}^{α}) and EC3 (C_{276}^{α}) was mounted on the template structures of the corresponding TM helices forming four separate segments of the 3D model of C5aR, namely, 38–63 (TM1), 71–138 (TM2 + EC1 + TM3), 150–224 (TM4 + EC2 + TM5), and 236–300 (TM6 + EC3 + TM7). Assembling of the complex between these segments and various fragments of C5a was performed as described above for building of the TM region, the difference being that energy minimization was performed in the space of $6 \times 5 = 30$ global parameters (three translations and three rotations for each of the four segments and for the fragment of C5a) instead of 42 global parameters in the case of the TM region. Typically, two types of energy calculations were performed for each configuration of the four C5aR segments and the fragment of C5a. The "simplified energy calculations" comprised energy minimization in the space of the global coordinates along with packing and repacking of spatial arrangements for each side chain at each convergence step of energy minimization by an algorithm developed previously (*40*). "Full-energy calculations" involved energy minimization not only within the space of global coordinates but also including the dihedral angles of the side chains.

RESULTS

C5aR. The TM region of human C5aR was modeled by homology with the X-ray structure of dark-adapted rhodopsin (the PDB entry 1F88) as described in the Materials and Methods section. The resulting 3D model differed from the rhodopsin TM region by the rms value of 2.4 Å and from the TM region of human β2-adrenergic receptor (the PDB entry 2RH1) by the rms value of 2.7 Å (C^{α} atoms only), which is close to the rms value of 2.0 Å calculated between the TM regions of rhodopsin (1F88) and β2-adrenergic receptor (2RH1). Then, the EC loops were restored and mounted on the 3D model of the TM region of C5aR. As described in the *Methods* section, our calculations revealed 29 possible conformations that differ from each other by an rms value of at least 3 Å (C^{α} atoms only). Finally, all 185 possible low-energy conformations of the N-terminal segment 8–41, which were obtained independently (see the Materials and Methods section), were mounted on the 3D model of the TM region of C5aR (on the TM1 residues 38–41), and those without steric clashes between the N-terminal segment and the rest of the model (corresponding $C^{\alpha}-C^{\alpha}$ distances ≥3 Å) were selected for further consideration. We also required that the conformation of a segment should not enter the membrane space (by visual inspection). Totally, 44 conformations of the N-terminal segment were included in the final 3D model of C5aR that consisted of the TM region, the EC loops, and the N-terminal segment.

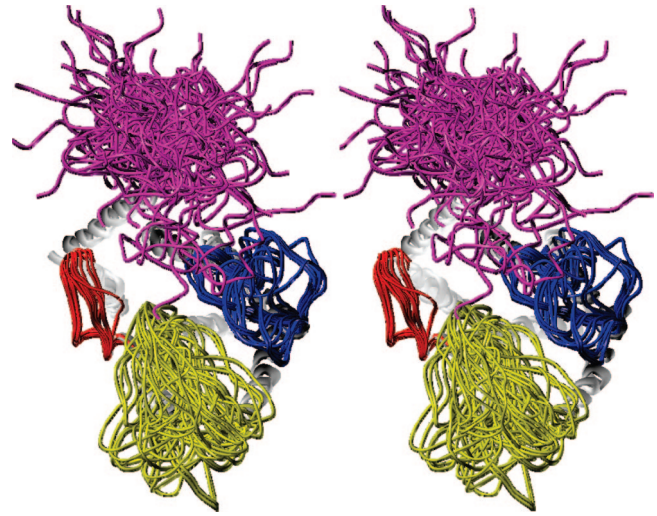

FIGURE 1: Stereoview of the 3D model of C5aR. Different possible conformations of the EC loops (29 conformations) and the N-terminal segment (44 conformations) are shown as tubes of different colors (EC1 in red, EC2 in yellow, EC3 in blue, and N-term in magenta). The TM region is shown as white shaded ribbons. The view is from the extracellular side roughly perpendicular to the membrane plane.

The resulting model is represented by the sketch in Figure 1, where different possible conformations of the EC loops and the N-terminal segment are shown as tubes. EC1 was the least flexible loop, and EC2 and EC3 were the most flexible ones. Possible movements of the "tips" of EC2 (C_{177}^{α}) and EC3 (C_{276}^{α}) within the sets of low-energy conformations were as large as 21.8 and 18.3 Å, respectively. In the closed modes, EC3 may almost completely block access of C5a to the cavity in the TM region between TM5, TM6, and TM7 where the second binding site was suggested; EC2 may block access to the same cavity only partially. Figure 1 also shows that most of the possible conformations of the N-terminal segment are not in direct contact with the EC loops, but some of them are located in the "capping" positions relative to the loops and also may partially cover the cavity in the TM region.

Strictly speaking, the resulting number of possible conformers of the N-terminal segment in the 3D model of C5aR and their distribution between possible spatial locations may depend on the specific modeling approach employed for a given molecular system. For instance, one can imagine additional MD simulations that include not only C5aR itself but also the lipid bilayer, explicit water molecules, etc. Such simulations starting from each of the combinations of the conformers of the EC loops (29 conformations) and the

N-terminal segment (44 conformations) might select more refined spatial arrangements among all 1276 combinations but would require exceptional computer resources. At the same time, the simple force field used in this study allowed selection of reasonable dynamic conformations for the EC loops and the N-terminal segment that successfully matches existing experimental data (see the Discussion section).

C5a. C5a consists of two segments that differ dramatically in conformational flexibility. The large N-terminal core is rigidified by three internal disulfide bridges, namely, between Cys21 and Cys47, Cys22 and Cys54, and Cys34 and Cys55. Two independent NMR studies revealed the same 3D structure of the core fragment 1–62, whereas the C-terminal 63–74 fragment displayed very different conformations (*2, 3*). Because the C-terminal fragment is extremely important for binding of C5a to C5aR, it was necessary to determine, or at least to suggest, possible conformation(s) that it may acquire in the C5aR/C5a complex. These conformations were deduced in our study for fragment C5a 59–74 by assuming that the conformation of the peptide backbone of the C5a 59–62 fragment was the same as in the NMR-derived structure (*3*) and the conformation of the fragment C5a 66–69 was the same as determined by the NMR studies of the rigid C5a agonist YSFKPMPLaR in different solvents (*41, 42*). The conformations of the fragments C5a 63–65 and C5a 70–74 were assumed to vary (see the Materials and Methods section, as well as the Supporting Information). Energy calculations suggested 30 different low-energy conformations of the fragment C5a 59–74. Obviously, not all of them were suitable for forming a stable complex of C5a with C5aR; however, all of them were explored from that perspective (see below).

Complex of C5a and C5aR. Building a 3D model of the complex of C5a and C5aR was achieved in several successive steps of selecting various orientations of the conformations of C5a within C5aR most suitable for establishing a stable complex. First, orientations of the C5a fragment 65–69 (in the single conformation deduced from the NMR studies of YSFKPMPLaR, see above) were sampled on the grid of the six global coordinates for this fragment defined as in the Materials and Methods section. The grid steps of translations were that of −2, 0, 2, and, in some cases, ±4 Å; and of rotations of −30, 0, and 30° for rotations *Y* and *Z* and from 0° to 330° over interval of 30° for rotation *X* (along the long axis of the fragment). We manually selected the reference point of the grid within the cavity between TM5, TM6, and TM7 of C5aR, which presumably contains the second binding site for C5a. In addition, the grid was placed at a level across the long axes of TM helices to accommodate the "outward" orientation of residue Asn64 when fragment 65–69 would be elongated (Asn64 in human C5a can be glycosylated (*43*); the N-linked glycosylation was not modeled in our study).

Simplified energy calculations performed for the TM region of C5aR with the C5a fragment 65–69 for each of the 5184 grid points yielded 76 orientations with the relative energy cutoff of 30 kcal/mol. Then, the "most open" conformation of the EC loops was mounted on the TM region (see the Materials and Methods section). Out of 76 selected orientations of the C5a fragment 65–69, 20 did not show steric clashes with the EC loops (corresponding $C^{\alpha}-C^{\alpha}$ distances ≥4 Å). These 20 orientations were combined with 30 low-energy conformations of the C5a fragment 59–74 obtained earlier (see above). Only 29 of the resulting 600 orientations of the C5a 59–74 fragment lacked steric clashes with either the TM region or the EC loops of C5aR (corresponding $C^{\alpha}-C^{\alpha}$ distances ≥3 Å). Simplified energy calculations performed for the complex of the TM region of C5aR and C5a 59–74 in all 29 orientations showed that 11 orientations could be considered as low-energy ones with relative energies lower than 60 kcal/mol. Only five of them, however, displayed a tendency to direct the N-terminal part of C5a toward the N-terminal segment of C5aR, where the first binding site for C5a was suggested. Therefore, only these five orientations were selected for further consideration.

The five selected orientations were subjected to full-energy calculations performed for the complex of four segments TM1, TM2 + EC1 + TM3, TM4 + EC2 + TM5, and TM6 + EC3 + TM7 (see the Materials and Methods section) and C5a 59–74. One of the orientations resulted in unavoidable steric clashes between side chains of EC3 and C5a 59–74 and was dropped from further considerations. The remaining four orientations, referred to as A, B, C, and D, showed reasonable energies ranging from −928 kcal/mol for A to −740 kcal/mol for D. At this step, however, no orientation was discarded despite the seemingly large difference in calculated energies. As it was noted already in connection with the 3D model of C5aR featuring different possibilities for the N-terminal segment, our modeling procedure did not consider the lipid bilayer and water environment of the extracellular part of C5aR. Especially important are the charged heads of phospholipids whose interaction with the charged side chains of the C5aR and C5a residues may significantly influence the relative energies corresponding to different orientations of C5a 59–74.

Next, the rigid core C5a 1–62 (from the PDB entry 1KJS) was overlapped to the fragment 59–62 in the obtained four orientations of C5a 59–74, and the resulting orientations of the entire C5a 1–74 were checked for possible steric overlap with C5aR. All four orientations of C5a did not clash (corresponding $C^{\alpha}-C^{\alpha}$ distances ≥3 Å), except orientation B, where an insignificant clash of C5a with EC1 was eliminated by a slight deviation in the C5a backbone (φ_{Leu61} was changed by 20°). Then, the 44 low-energy conformations of the N-terminal segment 8–41 of C5aR obtained independently (see above) were overlapped with residues 38–41 of TM1 in the complexes of C5aR/C5a (more exactly, the complexes of the fragments TM1, TM2 + EC1 + TM3, TM4 + EC2 + TM5, TM6 + EC3 + TM7, and C5a) corresponding to each of the four orientations of C5a. Thirty-seven conformations of the N-terminal segment of C5aR showed no steric clashes with C5a ($C^{\alpha}-C^{\alpha}$ distances ≥3 Å) for orientation A, 21 for B, 42 for C, and five for D. The obtained sets of conformations of the N-terminal segment of C5aR were considered as compatible to each orientation of C5a, respectively. Figure 2 depicts all four orientations of C5a within C5aR with all possible conformations of the N-terminal fragment of C5aR not clashing with C5a.

After that, available data of site-directed mutagenesis of C5a were used to evaluate the most plausible orientation of C5a in C5aR rather than selecting based on the energy differences between the four orientations of C5a 59–74. Red spheres in Figure 2 mark the residues in the rigid core C5a 1–62 that potentially involved in direct interactions with

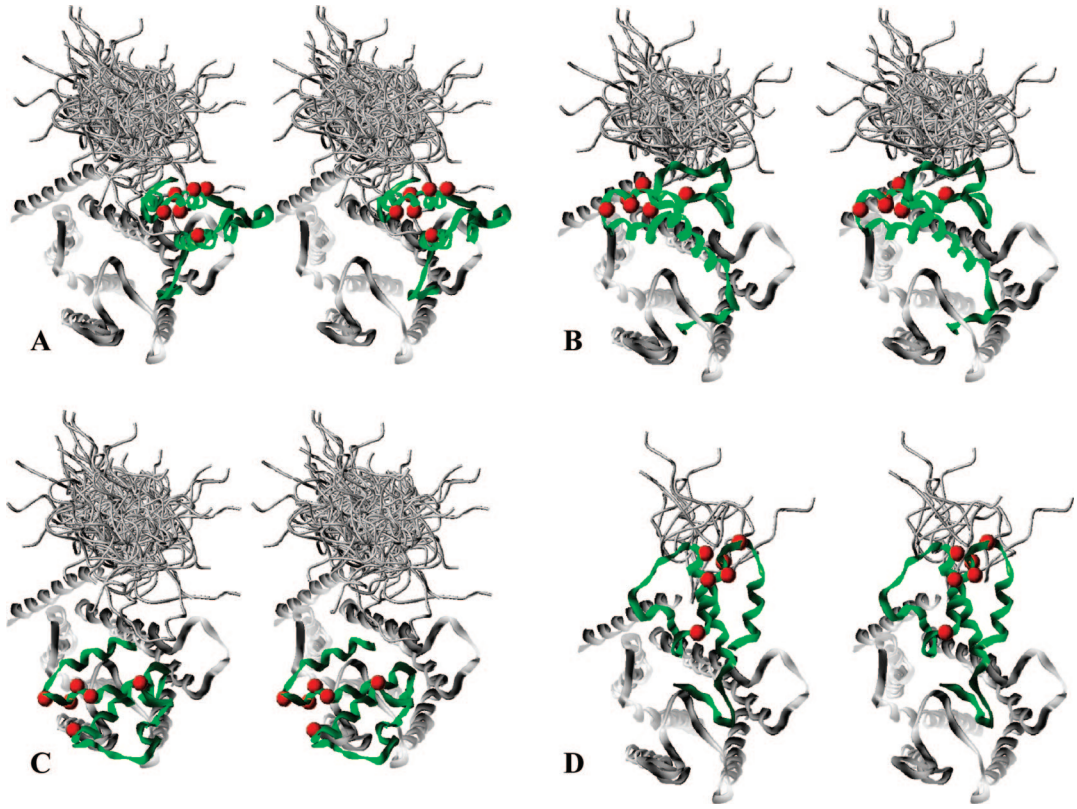

FIGURE 2: Stereoviews of the four possible orientations of C5a within C5aR. C5aR is shown as a white shadowed ribbon, except that the N-terminal segments are shown as white tubes. C5a is shown as a green shadowed ribbon. C5a residues His15, Val18, Lys19, Lys20, Cys 27, and Arg46 are marked by red spheres. Residues of C5a most distant (Ca−Ca distances >15 Å) from all residues of the compatible conformations of the N-terminal segment are as follows: Arg46 in panel A; His15, Val18, Lys19, Lys20, and Arg46 in panel C; and Cys27 in panel D.

C5aR according to experimental data of site-directed mutagenesis for C5a, namely, His15 (*17*), Val18 (*17*), Lys19 and Lys20 (*16, 17*), Cys 27 (*21*), and Arg46 (*17*) (briefly discussed in the Introduction). Calculation of $C^{\alpha}-C^{\alpha}$ distances showed that there was no single conformation of the N-terminal segment of C5aR that allowed all of the above residues of C5a to be located as close as 15 Å to any of the C5aR residues for all four orientations of C5a. However, because of the high flexibility of the N-terminal segment, at least one conformation from the set of the N-terminal segment conformations corresponding to orientation B allowed some of the C5aR residues to be located as close as 15 Å to all of the above residues of C5a. It was not the case for orientations A, C, and D. Specifically, residue Arg46 of C5a was not located close to any residue of any of the N-terminal segment conformations compatible for orientation A; the same was true for residues His15, Val18, Lys19, Lys 20, and Arg46 for orientation C and for residue Cys 27 for orientation D. This is clearly seen in Figure 2. In other words, the entire set of conformations of the N-terminal segment of C5aR compatible to orientation B may rationalize the experimental data of site-directed mutagenesis for C5a, whereas the sets of conformations of the N-terminal segment of C5aR compatible to orientations A, C, and D did not account for the set of potential interactions with essential residues in C5a ligand. Therefore, orientation B of C5a within C5aR was selected for a working hypothesis as the most plausible.

The B orientation of ligand–receptor complex assumed that the EC loops of C5aR were in the most open conformation, thus allowing the C-terminal fragment of C5a to be inserted into the cavity formed in C5aR by TM5, TM6, and TM7. However, it is possible that the C5a ligand binds to receptor conformations in which the EC loops are in more closed positions. Calculations of $C^{\alpha}-C^{\alpha}$ distances between the residues of the EC loops and C5a showed that 11 of 29 low-energy conformations obtained for the EC1 + EC2 + EC3 package did not possess steric clashes with C5a ($C^{\alpha}-C^{\alpha}$ distances ≥3 Å). All 11 of these conformations of the EC loops should be regarded as possible options for the EC loops in the complex of C5aR and C5a, as well as 21 low-energy conformations of the N-terminal segment of C5aR that were found compatible with orientation B of C5a (see above).

Finally, the resulting 3D model of the complex of C5aR and C5a obtained in this study combined the well-defined orientation of the peptide backbone of C5a within C5aR with a variety of possible conformations of the EC loops and the N-terminal segment of C5aR, accounting, therefore, for conformational flexibility of the extracellular part of C5aR. The C5a/C5aR model is represented by a sketch in Figure 3, which can be readily compared to Figure 1 that shows the resulting 3D model for C5aR. Comparison of the two figures clearly shows that binding of C5a to C5aR resulted in selection of C5aR conformations in which the EC2 and EC3 loops were further from each other and had fewer possible interactions with the N-terminal segment of C5aR.

DISCUSSION

First Binding Site. C5a Interacts with the Entire Set of Conformations of the N-Terminal Segment of C5aR. The experimental data of site-directed mutagenesis suggested that

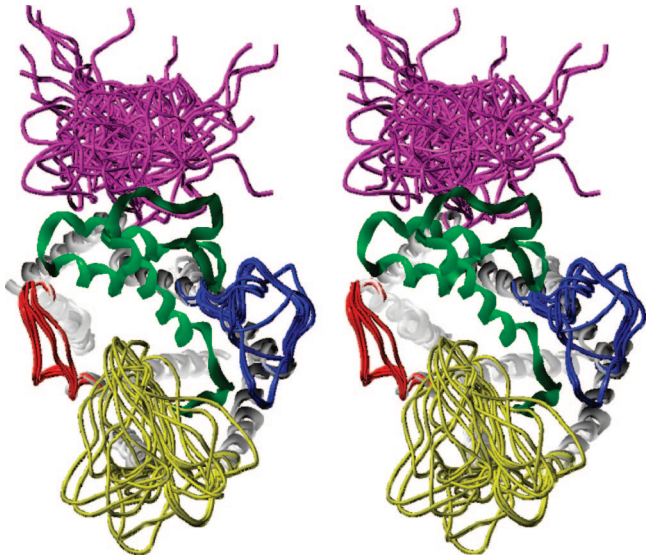

FIGURE 3: Stereoview of the resulting 3D model of the C5aR−C5a complex. C5a is shown as a green shadowed ribbon. Different possible conformations of the EC loops (29 conformations) and the N-terminal segment (21 conformations) are shown as tubes of different colors (EC1 in red, EC2 in yellow, EC3 in blue, and N-term in magenta). The TM region is shown as white shaded ribbons. The view is from the extracellular side roughly perpendicular to the membrane plane.

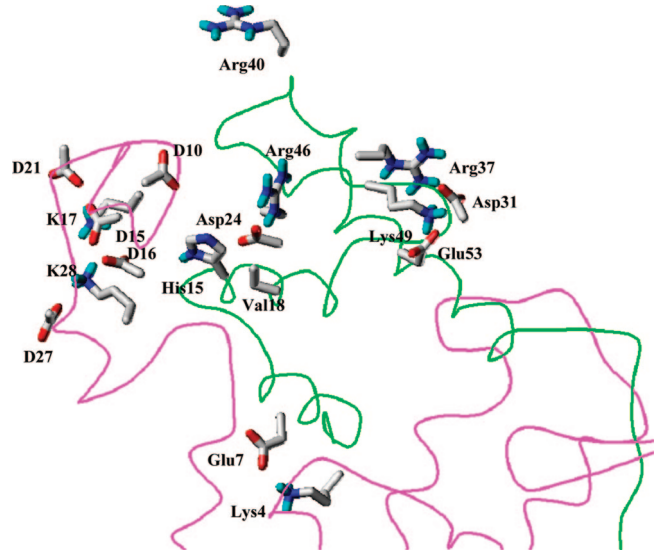

FIGURE 4: Sketch of conformation *q* in the C5aR−C5a complex. Backbone conformations are shown as magenta (C5aR) and green (C5a) one-line ribbons. Side chains of residues discussed in the text are shown as capped sticks and are labeled.

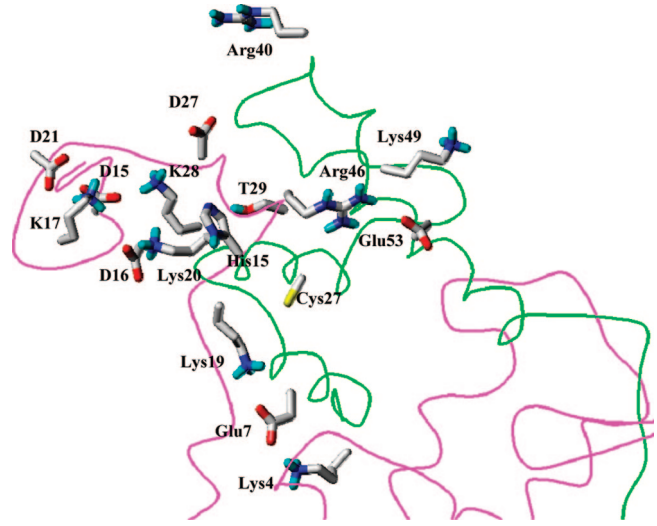

FIGURE 5: Sketch of conformation *j* in the C5aR−C5a complex. Backbone conformations are shown as magenta (C5aR) and green (C5a) one-line ribbons. Side chains of residues discussed in the text are shown as capped sticks and are labeled.

the first binding site of C5a within C5aR was located in the N-terminal segment, which is highly flexible. It is logical to assume that the entire set of low-energy conformations of the N-terminal segment of C5aR exists in dynamic equilibrium where different possible conformations interconvert between each other. Binding of C5a, as it was shown above, may influence the equilibrium by restricting the conformational possibilities (from 44 to 21 possible conformations) and, perhaps, by changing the interconversion rates but cannot reduce the set of low-energy conformations of the N-terminal segment to any single conformer. Clearly, different interconverting conformations of the N-terminal segment may interact with C5a during binding; therefore, the averaged effects observed by biological testing (for instance, decrease of binding level due to specific mutations in C5a or C5aR) should hardly be interpreted as an indication of interactions of specific residues of C5a with the same single conformation of the N-terminal segment of C5aR. In this regard, site-directed mutations in either the ligand or the receptor would change residue–residue interactions between C5a and the entire ensemble of conformations of the N-terminal segment of C5aR.

Considering the interaction of C5a with the entire set of low-energy conformations of the N-terminal segment of C5aR that are in dynamic equilibrium helped rationalize the experimental data obtained by site-directed mutagenesis. For 17 low-energy conformations of the N-terminal segment (out of 21 mentioned above), at least some of the residues were located in proximity ($C^{\alpha}-C^{\alpha}$ distances ≥ 10 Å) to at least one of the C5a residues His15, Val18, Lys19, Lys20, Cys27, and Arg46; see the selection of orientation B described above. These conformations are denoted further by letters from *a* to *q*. Simplified energy calculations were performed for the complex of five segments, namely, the N-terminal segment + TM1, TM2 + EC1 + TM3, TM4 + EC2 + TM5, TM6 + EC3 + TM7, and C5a, where the N-terminal segment possessed one of each conformations *a*–*q*. (Sketches of typical conformations, namely, *q* and *j*, are depicted in Figures 4 and 5, respectively.) Because of limitations of the modeling procedure discussed above, the main goal of these calculations was not to estimate the exact energy values corresponding to each case but rather to repack the side chains of the C5aR and C5a residues to allow analysis of residue–residue interactions between the N-terminal segment of C5aR and C5a as well as within both moieties.

Because both of the N-terminal segments of C5aR and C5a contain many residues with the charged side chains, the most important residue–residue interactions might be those allowing salt bridges between oppositely charged residues. Table 1 presents the systems of the salt bridges found by modeling for each of conformations *a*−*q* within C5aR, within C5a and between them. (The salt bridge was defined as a contact between the oppositely charged side chains where at least one of the distances between atoms belonging to the

Table 1: Systems of the Salt Bridges between Side Chains of C5aR and C5a Marked by Asterisks

	conformations of the N-terminal segment of C5aR																
contact	*a*	*b*	*c*	*d*	*e*	*f*	*g*	*h*	*i*	*j*	*k*	*l*	*m*	*n*	*o*	*p*	*q*
D15−K28	*			*						*							*
D15−K17	*	*	*	*	*	*	*	*	*	*	*	*	*	*	*	*	*
K17−D21	*			*		*	*	*		*	*	*	*		*	*	*
D16−K17		*	*		*	*	*	*	*			*	*	*	*	*	*
D21−K28		*															
D27−K28			*	*	*		*		*	*		*		*			*
D16−K28				*													*
Lys4−Glu7	*	*	*	*	*	*	*	*	*	*	*	*	*	*	*	*	*
Lys5−Glu8	*		*	*	*		*	*	*		*		*				
Asp31−Arg37	*	*	*	*	*	*	*	*	*		*	*	*	*	*	*	*
Lys20−Asp24		*	*				*		*			*	*		*		
Glu7−Lys19										*						*	
Lys49−Glu53	*	*	*	*	*		*	*	*					*	*		*
Arg46−Glu53		*	*			*	*	*	*	*	*	*	*		*	*	
Lys20−D18						*											
Lys19−D18								*									
Lys20−D16										*							
Lys20−D21														*			

corresponding side chains was less than 3.5 Å.) The systems of residue–residue contacts between the peptide backbones of C5a and the N-terminal segment of C5aR in conjunction with the salt bridges described in Table 1 can be directly used to rationalize the experimental data of site-directed mutagenesis targeting the first binding site of C5a in C5aR.

Rationalizing of the Available Experimental Data of Site-Directed Mutagenesis. Table 1 shows, for instance, that residues D15, D16, and D21 of C5aR are involved in the salt bridges with K17 in practically all conformations *a*−*q*. It implies that a decrease of affinity for C5a upon binding toward the C5aR mutants with simultaneous replacements of D15, D16, and D21 by alanines (*14*) or asparagines (*18*) was mainly due to interruptions of the salt bridges within the N-terminal segment of C5aR and, consequently, due to distortions in its conformations rather than due to interruption of interactions with C5a. (Note that the salt bridges D15−K17 and D21−K17 (or D16−K17) may still preserve the 3D shape of the N-terminal segment in conformation *j* (or *n*) where the side chains of D16 or D21 are redirected to interact with residue Lys20 in C5a.) At the same time, the reason why mutations D27N or (D21N, D27N) did not affect binding affinity of C5a (*18*) may be because D27 is involved in a less important salt bridge only with neighboring K28 and only in some conformations of the N-terminal segment of C5aR. D18 does not form salt bridges within C5aR but may interact with Lys19 or Lys 20 of C5a in conformations *f* and *h*, respectively, which may explain observed decrease of binding upon mutation of either (or both) of these residues to alanine (*16, 17*).

On the other hand, because residues His15, Val18, and Arg46 are located close to each other in the rigid core of C5a ($C_{15}^{\alpha}-C_{18}^{\alpha}$ distance being 5.3 Å, $C_{15}^{\alpha}-C_{46}^{\alpha}$ distance being 10.4 Å, and $C_{18}^{\alpha}-C_{46}^{\alpha}$ distance being 6.0 Å), one may suggest that mutations involving these residues (*17*) may be interdependent. In our view, most effects observed experimentally upon mutations of the above residues may be explained by the conformational flexibility of the relatively long side chain of Arg46 within C5a. When the side chain of Arg46 is directed toward the N-terminal segment of C5aR, possible favorable electrostatic interaction (although not that strong as a salt bridge) may occur between Arg46 and D10 (as, for instance, in conformation *q* depicted in Figure 4) or between Arg46 and D16 (as it may be possible in conformation *f*; not shown). If, however, the side chain of Arg46 is directed inward C5a or is replaced by alanine, those presumably important interactions may not occur. This may happen as a result of the single mutations Arg46Ala (17-fold decrease of affinity for C5a) or His15Ala (10-fold decrease), since elimination of the closely spaced side chain of His15 may destabilize the favorable spatial position of the side chain of Arg46 (the alternative explanation may be elimination of electrostatic interaction between His15 and D10). Similar explanations can account for the synergistic effects of the double mutation His15Ala, Arg46Ala (296-fold decrease in affinity for C5a). The possible movement of the side chain of Arg46 inward C5a may also be expected as a result of the mutations involving Lys49, such as (Leu43Ala, Lys49Ala) (23-fold decrease) and (His15Ala, Leu43Ala, Lys49Ala) (500-fold decrease). Indeed, the side chain of Glu53 may form a salt bridge either with Lys49 or with Arg46 (see Table 1; Figure 4 shows the case with the Lys49-Glu53 salt bridge); obviously, the possibility of forming an Arg46−Glu53 salt bridge is greatly increased when the competing side chain of Lys49 is eliminated. Similar reasoning can be used to rationalize the effects of another synergistic mutation (His15Ala, Leu43Ala, Arg46Ala, Lys49Ala, Glu53Ala); 4000-fold decrease in affinity. Also, the reduced affinity for C5a due to mutation Val18Asp (712-fold decrease) may be explained by formation of a strong salt bridge Asp18−Arg46, which also would result in moving the Arg46 side chain inward C5a, thus making it unavailable for interaction with the receptor.

Most of the data of the site-directed mutagenesis indicated residues that may be involved in the interface between C5a and the first binding site in C5aR belonging either to C5a (*16, 17*) or to C5aR (*14, 18*). Our study suggested that Cys27 of C5a might contact fragment 24–30 of C5aR (*21*), in general agreement with the independent NMR study (*19*). Interestingly, conformation *j* of the N-terminal segment of C5aR found by our modeling also provides for such contacts. Conformation *j* is depicted in Figure 5; the system of salt bridges characteristic for this conformation is described in Table 1. Unlike conformation *q* in Figure 4, this conformation of the N-terminal segment features the side chain of Lys20 directly involved in a salt bridge with D16 as well as the

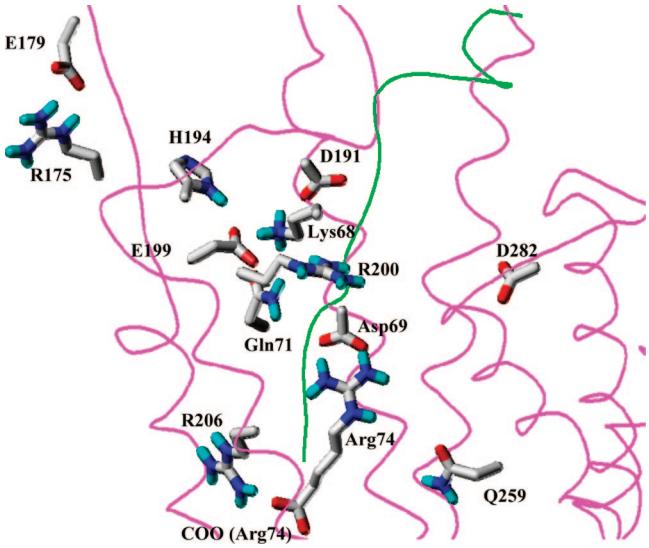

FIGURE 6: Sketch showing residue–residue interactions in the second binding site for C5a. Backbone conformations are shown as magenta (C5aR) and green (C5a) one-line ribbons. Side chains of residues discussed in the text are shown as capped sticks and are labeled.

side chain of Arg46 involved in a salt bridge with Glu53. In our view, these two examples, namely, conformations *j* and *q*, demonstrate how the flexible N terminus of C5aR might sample multiple potential interactions with the C5a ligand. Indeed, effects of replacements of Arg46, Glu53, and other residues discussed above in connection with conformation *q* would be difficult to explain based on conformation *j*; and vice versa, contacts suggested for Cys27 would be difficult to explain based on conformation *q*. However, the hypothesis that the experimental data reflect effects that are averaged over a set of interconverting conformations found by modeling allows rationalization of the wide variety of experimental observations.

Our very recent data based on the novel technique of disulfide trapping by random mutagenesis in yeast explored possible contacts between specific residues of C5a and specific regions of the N-terminal fragment of C5aR (*22*). It was shown that residues N23, T24, V26, and D27 of C5aR may interact with Cys24 in the C5a mutant [Asp24Cys, Cys27Arg]; G12 and Y14 with Cys15 in C5a [His15Cys, Cys27Arg]; G12, D15, T24, and V26 with Cys40 in C5a [Arg40Cys, Cys27Arg]; and S3 and Y6 with Cys46 in C5a [Arg46Cys, Cys27Arg] (*22*). These experimental data were not used in the process of building the 3D model of the C5a/C5aR complex described in the present study; however, they were in good agreement with the set of the conformations of the N-terminal fragment of C5aR proposed by modeling (see ref *22* for the detailed analysis).

Second Binding Site. While the systems of residue–residue interactions between C5a and the N-terminal segment of C5aR (in the first binding site for C5a) may differ from one conformation of the N-terminal segment to another, interactions between the C-terminal fragment of C5a and the second binding site in the TM region of C5aR were well-determined in the 3D model of the C5a/C5aR complex. Figure 6 presents a consistent picture of the residues involved in the most important interactions according to the model. The side chain of the Lys68 residue formed two strong salt bridges, one with the side chain of D191 in EC2 and another with the side chain of E199 in TM5. The spatial position of the E199 side chain was determined also by hydrogen bonding with the side chains of H194 in EC2 and Gln71 in C5a. Another important salt bridge was formed between the side chain of R206 in TM5 and the C-terminal carboxyl group of Arg74 in C5a. In Figure 6, the side chain of Asp69 was involved in the salt bridge with the side chain of Arg74; however, it may be easily switched to the equally strong salt bridge with the side chain of R200 in TM5. The side chain of D282 was located at some distance from C5a. A strong salt bridge was also formed between R175 and E179, both in EC2. According to our model, the side chains of fragment C5a 59–74 in the second site were contacted by the side chains of the following residues of C5aR: L117, M120, and Y121 in TM3; L167 and F172 in TM4; L187, C188, D191, and H194 in EC2; E199, R200, A203, R206, L207, L209, and P214 in TM5; M265 in TM6; and L277 and N279 in EC3 (a contact between the side chains was defined as an interatomic distance less than 4.5 Å). No contacts of C5a with the EC1 loops were found in agreement with the experimental data on side-directed mutagenesis (*30, 44*).

Rationalizing the Data on the C5aR Mutants E199K, D282R, R206A, and R175D. The model was further validated by focusing on residue–residue interactions between C5a and C5aR mutants E199K, D282R, R206A, and R175D. Simplified energy calculations for C5a fragment 65–69 within the TM regions of the mutants were performed using the same systematic search grid as was used for C5aR (see above). In all cases, similar results were obtained for low-energy orientations of the fragment C5a 65–69 as those depicted in Figure 6. This allowed full-energy calculations to be performed for C5a 59–74 fragment in the orientation displayed in Figure 6 within the mutants represented by the TM region and the EC loops as done earlier for C5aR. The most dramatic changes in residue–residue interactions occurred in the mutant E199K; the side chain of Lys68 was pushed away from the position that it occupied in Figure 6, and a strong salt bridge appeared between the side chains of K199 and D191. The side chain of D191 hydrogen bonded with the H194 side chain, and the hydrogen bonds that had existed between E199 and H194 and Gln71 in the case of C5aR were also broken; other interactions remained basically the same. According to calculations, mutant E199K lost ca. 60–70 kcal/mol in energy of interaction between C5a fragment 59–74 and the TM4 + EC2 + TM5 fragment of the receptor as compared to the same energy in the case of C5aR. This estimation depended on involvement of the side chain of Asp69 in the salt bridge either with Arg74 or with R200 as well as on other limitations of the modeling procedure noted above; however, it clearly shows that the second binding site in E199K does not favor binding of C5a. This finding agrees with the experimental observation of a 7-fold decrease in binding of C5a to E199R (*23*) and does not contradict the experimental data showing equally good binding of C5a to C5aR and E199Q (*24*), since in the latter case the salt bridges formed by E199 may be replaced by corresponding hydrogen bonds. At the same time, the levels of biological response, which is the complex reaction where ligand binding is only an initial stage, were close to those of C5aR for E199K (*25*) or E199R (*23*). Marked discrepancies between levels of C5a binding and biological response for C5aR mutants with replacements of E199, D282, and

R206 were repeatedly observed (see, for example, ref *1*); therefore, only the experimental data on C5a binding were considered.

Modeling showed minimal changes in residue–residue interactions between C5a and the receptor in the case of D282R; the modest loss in energy of interaction between C5a fragment 59–74 and the TM6 + EC3 + TM7 fragment of the receptor was ca. 20–25 kcal/mol. D282R showed a 4-fold decrease of binding to C5a (*27*), that is, less than that observed for E199R. Although we did not specifically model binding of C5a to the D282A mutant, we would expect no changes in this mutant as compared to C5aR.

No major changes were found in the system of residue–residue interactions between C5a and the R206A mutant receptor, except an obvious loss of the strong interaction between the side chain of R206 and the C-terminal carboxyl group of Arg74 in C5a and interruption of the hydrogen bonding between E199 and Gln71. The available experimental data on affinity of C5a toward R206A vary reporting either the same affinity as shown for C5aR (*28*), 3-fold (*29*) or 7-fold (*27*) decrease of affinity, or even complete absence of binding (*26*). The latter experimental observation does not fit the modeling results, while the two former data are in good agreement. No changes in interactions between C5a and the receptor were found also for the R175D mutant; however, the strong salt bridge between the side chains of R175 and E179 was predictably broken. Both R175 and E179 do not participate directly in interaction on the C5a/C5aR interface, but their interaction may be important for stabilization of the particular conformation of the EC2 loop corresponding to the "most open" structure. Accordingly, significant decreases in C5a binding to R175D and R175A [ca. 150-fold and 30-fold, respectively (*29*)] may be attributed to possible redistribution of the low-energy conformations in the EC1 + EC2 + EC3 package that would disfavor the most open conformer of the EC2 loop.

Exploring Interactions between E199 in C5aR and Lys68 in C5a. In the model shown in Figure 6, the salt bridge between the side chains of E199 in TM5 and Lys68 in C5a is an important stabilizing element of the C5aR/C5a complex. It implies that switching the side chains in a reciprocal mutation should not destabilize the complex and predicts that the affinity of the C5a [Lys68Glu] analogue to the E199K mutant should be close to that for binding C5a to C5aR. Indeed, this was observed experimentally for the C5a [Lys68Glu] analogue and the E199R mutant; the same study found that binding of C5a to E199R or C5a [Lys68Glu] to C5aR was only decreased 7-fold (*23*). We performed further modeling of this interaction that showed that differences in the system of residue–residue interactions between C5a [Lys68Glu] and E199R as compared to that depicted in Figure 6 are more complex than just replacing the salt bridge Lys68−E199 with Glu68−R199. First, low-energy conformations of the fragment C5a [Lys68Glu] 59–74 were calculated by the same procedure as for C5a 59–74 (see the Materials and Methods section) and clustered into 23 different clusters. [It was once again assumed that the backbone conformations of fragment 66–69 in C5a [Lys68Glu] may be deduced from the NMR structure of the C5a agonist YSFKPMPLaR (*41, 42*); the assumption is additionally justified by similarity of binding affinities of YSF**K**PMPLaR toward C5aR and YSF**E**PMPLaR toward E199R observed

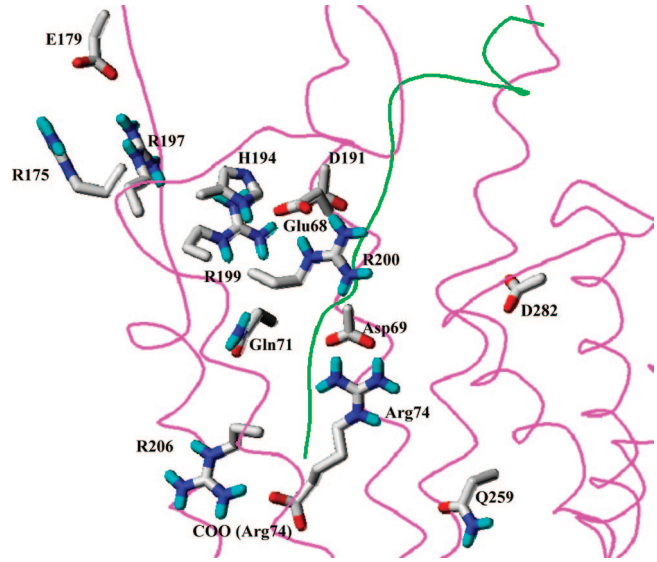

FIGURE 7: Sketch showing residue–residue interactions in the second binding site for C5a [Lys68Glu] interacting with E199R. Backbone conformations are shown as magenta (C5aR) and green (C5a) one-line ribbons. Side chains of residues discussed in the text are shown as capped sticks and are labeled.

experimentally (*45*).] Then, simplified energy calculations for C5a [Lys68Glu] fragment 65–69 within the TM region of E199R were performed exactly as for C5aR and the mutants discussed above. The calculations confirmed that C5a [Lys68Glu] possessed low-energy orientations of the fragment 65–69 in E199R very similar to the orientation of C5a 65–69 fragment in C5aR found by our model.

We then performed full-energy calculations for C5a [Lys68Glu] 59–74 fragment in this particular orientation within E199R represented by the TM region and the EC loops. The resulting structure is presented in Figure 7. As was expected, the salt bridge E199−Lys68 that stabilizes the C5aR/C5a complex was replaced by the R199−Glu68 one. That was not the only difference: A novel stabilizing element between C5a [Lys68Glu] and C5aR, the salt bridge R200−Glu68, appeared as well, replacing the salt bridge D191−Lys68 (the side chain of D191 switched to form the salt bridge with R199). The hydrogen bonding that formed the side chains of H194 and Gln71 with the side chain of E199 was obviously lost upon replacement of E199 to R199. At the same time, an additional positive charge of R199 pushed the side chain of R197 forming a salt bridge with the side chain of E179. As compared to the model of C5a 59–74 and C5aR, the energy of interaction between C5a [Lys68Glu] fragment 59–74 and the TM6 + EC3 + TM7 fragment of E199R was more preferable by ca. 60–80 kcal/mol.

C5a-des74 Binding to C5aR and Mutants. We also modeled the interactions of the truncated analogue C5a-des74 with C5aR mutated at E199 by R199 (or K199), since these interactions had been examined experimentally (*23*). The metabolite C5a-des74 is a less potent partial agonist of C5aR with ca. 30-fold decrease of affinity toward C5aR as compared to that of C5a (*27*). Contrary to what was observed with C5a, the level of binding of C5a-des74 toward WT and E199R was about the same as the level of binding of C5a-des74 [Lys68Glu] to E199R (*23*). Also, C5a-des74 equally well displaced the labeled C5a from binding to WT and

E119K, whereas C5a-des74 [Lys68Glu] displaced the labeled C5a much better in case of E199K than of WT (*23*). These observations led to the conclusion that C5a-des74 might have a different binding mode to C5aR than the full-length C5a (*23*). Our modeling results both confirm and rationalize this conclusion. Full-energy calculations for C5a-des74 59–73 fragment in the same orientation as that of the C5a fragment 59–74 in the model of Figure 6 were performed within C5aR. The resulting system of residue–residue interactions was essentially the same as in Figure 6 except for two important elements, namely, the absence of the salt bridge between the side chain of R206 and the C-terminal carboxyl group of Arg74 and involvement of the side chain of Asp69 in the strong salt bridge with the side chain of R200. Therefore, if C5a des-74 binds to the second site of C5aR in the same mode as the full-length C5a, the system of interactions should be disturbed by replacement of E199 by R199, and binding affinity of C5a-des74 to E199R should be decreased; however, this was not observed experimentally (*23*). Independently, when we sampled orientations of the low-energy conformations of C5a-des74 fragment 59–73 within the TM region of C5aR, we did not find orientations similar to that of C5a fragment 65–69 in the original model displayed in Figure 6. Taken together, these two findings strongly suggest that the C-terminal fragment of C5a-des74 may bind to the C5aR in a different orientation than does C5a.

Recent studies of the orphan receptors C5L2 from different species, which bind both C5a and C5a-des74 with high affinity, provide additional independent evidence in favor of different binding modes for C5a and C5a-des74 (*46, 47*). As discussed above, if the binding modes of both C5a and C5a-des74 to C5aR are similar to that in Figure 6, the strong salt bridge between the side chains of Asp69 and R200 becomes the important element of stabilization of the C5aR/C5a-des74 complex. This element would not exist in the complex of C5L2 and C5a-des74, since R200 in C5aR corresponds to N198 in human C5L2 or to V204 in mouse and rat C5L2s (according to the multiple sequence alignment performed by CLUSTAL W; data not shown). Therefore, one might expect that if the binding modes of both C5a and C5a-des74 to C5L2 are similar to that in Figure 6, affinity of C5a-des74 to C5L2 would decrease as compared to that of C5a contrary to experimental observations (*47*).

The model from this study also predicts that the binding of intact C5a to C5aR may be different than that of C-terminal fragments of C5a and their analogues. For instance, a docking model for C5a hexapeptide antagonist ChaW (Me-Phe-Lys-Pro-D-Cha-Trp-D-Arg, D-Cha is D-cyclohexylalanine) identified residues I116 in TM3, R206 in TM5, and V286 in TM7 as those involved in direct interaction with ChaW and, additionally, postulated involvement of the aromatic residues Y121 (TM3), F211 (TM5), F251, W255, and Y258 (all in TM6) in the interaction with the side chain of D-Arg in ChaW (*31*); only two of these residues, namely, Y121 and R206, were listed as those contacting C5a in our model (see above). Another docking model for the cyclic hexapeptide antagonist of C5a, Phe-*cyclo*(Orn-Pro-D-Cha-Trp-Arg), suggested contacts of this molecule with I116 in TM3, R175 in EC2, E199 and R206 in TM5, Y258 in TM6 and D282, and V286 in TM7 (*29*); again, only two residues, E199 and R206, were implicated in binding C5a in our model.

Concluding Remarks. In this study, we modeled the 3D structure of the physiologically important C5a receptor bound to its natural polypeptide ligand, C5a. The modeling confirmed the previously suggested "two-site" model for binding C5a to C5aR that included the first site of interactions between the rigid core of C5a and the N-terminal segment of C5aR and the second site involving interactions of the TM region of C5aR and the C-terminal fragment of C5a. The modeling results showed that there are two fundamentally very different ways of interacting of C5a and C5aR at the two sites. The C-terminal fragment of C5a and the TM region of C5aR (the second site) interacted through a well-determined system of the strong salt bridges and hydrogen bonding between specific side chains; the most important interactions were those between E199 and Lys68, D191 and Lys68, and R206 and the C-terminal carboxyl group of Arg74. This system of interactions was achieved by conformational adjustment of the flexible C-terminal fragment of the ligand to the relatively rigid structure of the TM bundle of the receptor immobilized within the membrane. In contrast, interactions between the N-terminal segment of C5aR and the rigid core of C5a (the first site) varied depending on conformations of the highly flexible N-terminal segment of C5aR. Accordingly, the receptor conformations adjusted to the rigid core of the ligand. Our modeling predicts multiple conformations of the flexible N terminus of the C5aR, which together corroborate available experimental data of site-directed mutations of the N-terminal segment of C5aR.

Currently available experimental data on binding affinities for the various analogues of C5a and the mutants of C5a obtained by the site-directed mutagenesis were successfully rationalized using the 3D model of the C5aR/C5a complex, thus significantly validating the model. The model also rationalized the very recent data by the novel technique of disulfide trapping by random mutagenesis in yeast (*22*) that was obtained after the model was built. Also, the modeling results predicted that full-length C5a and C5a-des74 metabolite may have different binding modes with C5aR explaining discrepancies in the corresponding experimental data related not only to C5aR but also to the C5L2 receptors from different species. Along the same lines, binding modes of linear and cyclic hexapeptide antagonists of C5a toward C5aR were also predicted to be different from that of C5a.

It is also noteworthy that the proposed 3D model relates to the specific step of interaction between C5a and C5aR, namely, to forming the initial binding complex between the two molecules. At this step, C5aR still exists in the resting state, which allows modeling of the structure of the TM region of C5aR by homology with the dark-adapted structure of rhodopsin. However, further steps, such as receptor activation, would require conformational changes in C5aR not known presently, so the structure of C5aR corresponding to the activated state cannot be modeled in the same way as the structure of the resting state. For rhodopsin, for instance, the two very different 3D models for the activated state of the TM region were proposed based either on the crystallographic data (*48*) or on the data of site-directed spin labeling (SDSL) (*49*). Thus, rationalization of the experimental data of site-directed mutagenesis in C5aR related to receptor activation may be difficult in terms of the 3D model proposed in our study.

Our study also has implications extending to modeling docked structures for entire family of GPCRs and polypeptide ligands. First, our procedure of docking a ligand within a receptor did not use any direct experimental constraints derived from site-directed mutagenesis of GPCRs or from partial structural data (such as incorporation of the Zn^{2+} binding sites) used in many recent modeling studies (for instance, for docking opioid peptides in various opioid receptors (*50*), nonpeptide and peptide agonists in human melanocortin-4 receptor (*51*), angiotensin II in the angiotensin receptors of type 1 (*52, 53*) and type 2 (*54*)). In fact, we performed "almost de novo" modeling where only two main assumptions derived from experiment were used. Specifically, we selected a reference point for a systematic grid search for placement of C5a fragments within the cavity between TM helices of C5aR that involved residues E199, R206, and D282; and we selected only the orientations of C5a capable of interaction with the N-terminal segment of C5aR, specifically with the six residues, His15, Val18, Lys19, Lys20, Cys 27, and Arg46 (see Figure 2). This strategy reserved the bulk of site-directed mutagenesis data for independent validation of the predicted conformations of docked ligand and receptor.

Second, our modeling procedure was the first to directly take into account various conformational possibilities of the flexible EC loops and the N-terminal segment of GPCRs. This is especially important in view of the very recent experimental findings that clearly showed dramatic differences between conformations of the EC2 loop in dark-adapted rhodopsin and human β2-adrenergic receptor. As a rule, the 3D models of GPCRs used for modeling interactions between the receptor and the peptide ligand were limited to the TM regions (e.g., docking of angiotensin II to the angiotensin receptor of type 1 (*39, 55*), cyclopentapeptide ligands to CXCR4 receptor (*56*), and vasopressin-related peptides to vasopressin and oxytocin receptors (*57*)). Otherwise, only single conformations for the EC loops and/or the N-terminal segment of C5aR were included in models (*50, 51, 53, 58*). As an exception to this, a recent paper reported docking angiotensin II to the most open conformation of the EC loops selected from the large set of options modeled for the type 2 angiotensin receptor (*54*). The present study successfully considered a variety of low-energy conformations for the EC loops and the N-terminal segment of C5aR to rationalize the experimental data related to interactions of the rigid core of C5a with the highly flexible N-terminal segment. Undoubtedly, modeling procedures developed to account for flexibility of the extracellular part of C5aR should also be applicable for studies of molecular mechanisms of binding of many polypeptide ligands to their specific receptors [e.g., the suggested "two-site" binding of chemokine CXCL12 to the CXCR4 receptor (*59*)].

Third, because we considered various conformational possibilities for the EC loops and the N-terminal segment of C5aR, our 3D model of the C5aR and C5a predicts molecular mechanisms that may be common for recognition of peptide ligands by their specific GPCRs. For instance, it is widely accepted that forming the ligand–receptor complex is associated with "induced fit" of the flexible ligand to the more rigid receptor. Our modeling results, however, pointed out that both components of the system can be involved in "mutual induced fit", where the interface between the molecules is determined both by the receptor selecting the proper conformation(s) of the ligand (interactions between the TM region of C5aR and the C-terminal fragment of C5a) and by the ligand selecting the proper conformation(s) of the receptors (interactions between the rigid core of C5a and the N-terminal segment of C5aR). Furthermore, the results allow speculation on possible dynamics of "chaperoning" C5a to the proper orientation relative to C5aR via successive contacts with various conformations of the N-terminal segment of C5aR from the more extended outward from the membrane to more folded ones.

ACKNOWLEDGMENT

We thank Dr. Leo Kinarsky (University of Nebraska Medical Center) for providing the unpublished data on the 3D model of the C5a agonist YSFKPMPLaR derived from NMR measurements.

SUPPORTING INFORMATION AVAILABLE

Technical details of computational procedures related to the force field employed, to build-up procedures for C5a 59–74 and C5aR 8–41, and to restoring the EC loops. General outline of steps for building the complex of C5a and C5aR (Table S1). This material is available free of charge via the Internet at http://pubs.acs.org.

REFERENCES

1. Allegretti, M., Moriconi, A., Beccari, A. R., Di Bitondo, R., Bizzarri, C., Bertini, R., and Colotta, F. (2005) Targeting C5a: Recent advances in drug discovery. *Curr. Med. Chem. 12*, 217–236.
2. Zuiderweg, E. R., Nettesheim, D. G., Mollison, K. W., and Carter, G. W. (1989) Tertiary structure of human complement component C5a in solution from nuclear magnetic resonance data. *Biochemistry 28*, 172–185.
3. Zhang, X., Boyar, W., Toth, M. J., Wennogle, L., and Gonnella, N. C. (1997) Structural definition of the C5a C terminus by two-dimensional nuclear magnetic resonance spectroscopy. *Proteins 28*, 261–267.
4. Palczewski, K., Kumasaka, T., Hori, T., Behnke, C. A., Motoshima, H., Fox, B. A., Le Trong, I., Teller, D. C., Okada, T., Stenkamp, R. E., Yamamoto, M., and Miyano, M. (2000) Crystal structure of rhodopsin: A G protein-coupled receptor. *Science 289*, 739–745.
5. Teller, D. C., Okada, T., Behnke, C. A., Palczewski, K., and Stenkamp, R. E. (2001) Advances in determination of a high-resoultion three-dimensional structure of rhodpsin, a model of G-protein-coupled receptors (GPCRs). *Biochemistry 40*, 7761–7772.
6. Okada, T., Fujiyoshi, Y., Silow, M., Navarro, J., Landau, E. M., and Shichida, Y. (2002) Functional role of internal water molecules in rhodopsin revealed by X-ray crystallography. *Proc. Natl. Acad. Sci. U.S.A. 99*, 5982–5987.
7. Okada, T., Sugihara, M., Bondar, A. N., Elstner, M., Entel, P., and Buss, V. (2004) The retinal conformation and its environment in rhodopsin in light of a new 2.2 A crystal structure. *J. Mol. Biol. 342*, 571–583.
8. Li, J., Edwards, P. C., Burghammer, M., Villa, C., and Schertler, G. F. (2004) Structure of bovine rhodopsin in a trigonal crystal form. *J. Mol. Biol. 343*, 1409–1438.
9. Rasmussen, S. G., Choi, H. J., Rosenbaum, D. M., Kobilka, T. S., Thian, F. S., Edwards, P. C., Burghammer, M., Ratnala, V. R., Sanishvili, R., Fischetti, R. F., Schertler, G. F., Weis, W. I., and Kobilka, B. K. (2007) Crystal structure of the human beta2 adrenergic G-protein-coupled receptor. *Nature 450*, 383–387.
10. Cherezov, V., Rosenbaum, D. M., Hanson, M. A., Rasmussen, S. G., Thian, F. S., Kobilka, T. S., Choi, H. J., Kuhn, P., Weis, W. I., Kobilka, B. K., and Stevens, R. C. (2007) High-resolution crystal structure of an engineered human beta2-adrenergic G protein-coupled receptor. *Science 318*, 1258–1265.

11. Drews, J. (2000) Drug discovery: A historical perspective. *Science 287*, 1960–1964.
12. Mollison, K. W., Mandecki, W., Zuiderweg, E. R., Fayer, L., Fey, T. A., Krause, R. A., Conway, R. G., Miller, L., Edalji, R. P., and Shallcross, M. A. (1989) Identification of receptor-binding residues in the inflammatory complement protein C5a by site-directed mutagenesis. *Proc. Natl. Acad. Sci. U.S.A. 86*, 292–296.
13. Siciliano, S. J., Rollins, T. E., DeMartino, J., Konteatis, Z., Malkowitz, L., Van Riper, G., Bondy, S., Rosen, H., and Springer, M. S. (1994) Two-site binding of C5a by its receptor: An alternative binding paradigm for G protein-coupled receptors. *Proc. Natl. Acad. Sci. U.S.A. 91*, 1214–1218.
14. DeMartino, J. A., Van Riper, G., Siciliano, S. J., Molineaux, C. J., Konteatis, Z. D., Rosen, H., and Springer, M. S. (1994) The amino terminus of the human C5a receptor is required for high affinity C5a binding and for receptor activation by C5a but not C5a analogs. *J. Biol. Chem. 269*, 14446–14450.
15. Kawai, M., Quincy, D. A., Lane, B., Mollison, K. W., Luly, J. R., and Carter, G. W. (1991) Identification and synthesis of a receptor binding site of human anaphylatoxin C5a. *J. Med. Chem. 34*, 2068–2071.
16. Bubeck, P., Grotzinger, J., Winkler, M., Kohl, J., Wollmer, A., Klos, A., and Bautsch, W. (1994) Site-specific mutagenesis of residues in the human C5a anaphylatoxin which are involved in possible interaction with the C5a receptor. *Eur. J. Biochem. 219*, 897–904.
17. Toth, M. J., Huwyler, L., Boyar, W. C., Braunwalder, A. F., Yarwood, D., Hadala, J., Haston, W. O., Sills, M. A., Seligmann, B., and Galakatos, N. (1994) The pharmacophore of the human C5a anaphylatoxin. *Protein Sci. 3*, 1159–1168.
18. Mery, L., and Boulay, F. (1994) The NH_2-terminal region of C5aR but not that of FPR is critical for both protein transport and ligand binding. *J. Biol. Chem. 269*, 3457–3463.
19. Chen, Z., Zhang, X., Gonnella, N. C., Pellas, T. C., Boyar, W. C., and Ni, F. (1998) Residues 21–30 within the extracellular N-terminal region of the C5a receptor represent a binding domain for the C5a anaphylatoxin. *J. Biol. Chem. 273*, 10411–10419.
20. Farzan, M., Schnitzler, C. E., Vasilieva, N., Leung, D., Kuhn, J., Gerard, C., Gerard, N. P., and Choe, H. (2001) Sulfated tyrosines contribute to the formation of the C5a docking site of the human C5a anaphylatoxin receptor. *J. Exp. Med. 193*, 1059–1066.
21. Hagemann, I. S., Narzinski, K. D., Floyd, D. H., and Baranski, T. J. (2006) Random mutagenesis of the complement factor 5a (C5a) receptor N terminus provides a structural constraint for C5a docking. *J. Biol. Chem. 281*, 36783–36792.
22. Hageman, I. S., Miller, D. L., Klco, J. M., Nikiforovich, G. V., and Baranski, T. J. (2008) Structure of the complement factor 5a (C5a) receptor/ligand complex studied by disulfide trapping and molecular modeling, *J. Biol. Chem.* E-publication ahead of print: PMID 18195008.
23. Crass, T., Bautsch, W., Cain, S. A., Pease, J. E., and Monk, P. N. (1999) Receptor activation by human C5a des Arg74 but not intact C5a is dependent on an interaction between Glu199 of the receptor and Lys68 of the ligand. *Biochemistry 38*, 9712–9717.
24. Monk, P. N., Barker, M. D., Partridge, L. J., and Pease, J. E. (1995) Mutation of glutamate 199 of the human C5a receptor defines a binding site for ligand distinct from the receptor N terminus. *J. Biol. Chem. 270*, 16625–16629.
25. Cain, S. A., Higginbottom, A., and Monk, P. N. (2003) Characterisation of C5a receptor agonists from phage display libraries. *Biochem. Pharmacol. 66*, 1833–1840.
26. Raffetseder, U., Roper, D., Mery, L., Gietz, C., Klos, A., Grotzinger, J., Wollmer, A., Boulay, F., Kohl, J., and Bautsch, W. (1996) Site-directed mutagenesis of conserved charged residues in the helical region of the human C5a receptor. Arg2O6 determines high-affinity binding sites of C5a receptor. *Eur. J. Biochem. 235*, 82–90.
27. Cain, S. A., Coughlan, T., and Monk, P. N. (2001) Mapping the ligand-binding site on the C5a receptor: arginine74 of C5a contacts aspartate282 of the C5a receptor. *Biochemistry 40*, 14047–14052.
28. DeMartino, J. A., Konteatis, Z. D., Siciliano, S. J., Van Riper, G., Underwood, D. J., Fischer, P. A., and Springer, M. S. (1995) Arginine 206 of the C5a receptor is critical for ligand recognition and receptor activation by C-terminal hexapeptide analogs. *J. Biol. Chem. 270*, 15966–15969.
29. Higginbottom, A., Cain, S. A., Woodruff, T. M., Proctor, L. M., Madala, P. K., Tyndall, J. D., Taylor, S. M., Fairlie, D. P., and Monk, P. N. (2005) Comparative agonist/antagonist responses in mutant human C5a receptors define the ligand binding site. *J. Biol. Chem. 280*, 17831–17840.
30. Cain, S. A., Woodruff, T. M., Taylor, S. M., Fairlie, D. P., Sanderson, S. D., and Monk, P. N. (2001) Modulation of ligand selectivity by mutation of the first extracellular loop of the human C5a receptor. *Biochem. Pharmacol. 61*, 1571–1579.
31. Gerber, B. O., Meng, E. C., Dotsch, V., Baranski, T. J., and Bourne, H. R. (2001) An activation switch in the ligand binding pocket of the C5a receptor. *J. Biol. Chem. 276*, 3394–3400.
32. Nikiforovich, G. V., and Marshall, G. R. (2005) Modeling flexible loops in the dark-adapted and activated states of rhodopsin, a prototypical G-protein coupled receptor. *Biophys. J. 89*, 3780–3789.
33. Matsumoto, M. L., Narzinski, K., Kiser, P. D., Nikiforovich, G. V., and Baranski, T. J. (2007) A comprehensive structure-function map of the intracellular surface of the human C5a receptor. I. Identification of critical residues. *J. Biol. Chem. 282*, 3105–3121.
34. Nikiforovich, G. V., Taylor, C. M., and Marshall, G. R. (2007) Modeling of the complex between transducin and photoactivated rhodopsin, a prototypical G-protein-coupled receptor. *Biochemistry 46*, 4734–4744.
35. Dunfield, L. G., Burgess, A. W., and Scheraga, H. A. (1978) Energy parameters in polypeptides. 8. Empirical potential energy algorithm for the conformational analysis of large molecules. *J. Phys. Chem. 82*, 2609–2616.
36. Nemethy, G., Pottle, M. S., and Scheraga, H. A. (1983) Energy parameters in polypeptides. 9. Updating of geometrical parameters, nonbonded interactions, and hydrogen bond interactions for the naturally occuring amino acids. *J. Phys. Chem. 87*, 1883–1887.
37. Nikiforovich, G. V. (1994) Computational molecular modeling in peptide design. *Int. J. Pept. Protein Res. 44*, 513–531.
38. Gerard, C., and Gerard, N. P. (1994) C5A anaphylatoxin and its seven transmembrane-segment receptor. *Annu. Rev. Immunol. 12*, 775–808.
39. Nikiforovich, G. V., Zhang, M., Yang, Q., Jagadeesh, G., Chen, H. C., Hunyady, L., Marshall, G. R., and Catt, K. J. (2006) Interactions between conserved residues in transmembrane helices 2 and 7 during angiotensin AT1 receptor activation. *Chem. Biol. Drug Des. 68*, 239–249.
40. Nikiforovich, G. V., Hruby, V. J., Prakash, O., and Gehrig, C. A. (1991) Topographical requirements for delta-selective opioid peptides. *Biopolymers 31*, 941–955.
41. Finch, A. M., Vogen, S. M., Sherman, S. A., Kirnarsky, L., Taylor, S. M., and Sanderson, S. D. (1997) Biologically active conformer of the effector region of human C5a and modulatory effects of N-terminal receptor binding determinants on activity. *J. Med. Chem. 40*, 877–884.
42. Vogen, S. M., Prakash, O., Kirnarsky, L., Sanderson, S. D., and Sherman, S. A. (1999) Determination of structural elements related to the biological activities of a potent decapeptide agonist of human C5a anaphylatoxin. *J. Pept. Res. 54*, 74–84.
43. Fernandez, H. N., and Hugli, T. E. (1978) Primary structural analysis of the polypeptide portion of human C5a anaphylatoxin. Polypeptide sequence determination and assignment of the oligosaccharide attachment site in C5a. *J. Biol. Chem. 253*, 6955–6964.
44. Klco, J. M., Nikiforovich, G. V., and Baranski, T. J. (2006) Genetic analysis of the first and third extracellular loops of the C5a receptor reveals an essential WXFG motif in the first loop. *J. Biol. Chem. 281*, 12010–12019.
45. Vogen, S. M., Finch, A. M., Wadi, S. K., Thatcher, J., Monk, P. N., Taylor, S. M., and Sanderson, S. D. (1999) The influence of Lys68 in decapeptide agonists of C5a on C5a receptor binding, activation and selectivity. *J. Pept. Res. 53*, 8–17.
46. Cain, S. A., and Monk, P. N. (2002) The orphan receptor C5L2 has high affinity binding sites for complement fragments C5a and C5a des-Arg(74). *J. Biol. Chem. 277*, 7165–7169.
47. Scola, A. M., Higginbottom, A., Partridge, L. J., Reid, R. C., Woodruff, T., Taylor, S. M., Fairlie, D. P., and Monk, P. N. (2007) The role of the N-terminal domain of the complement fragment receptor C5L2 in ligand binding. *J. Biol. Chem. 282*, 3664–3671.
48. Salom, D., Lodowski, D. T., Stenkamp, R. E., Le Trong, I., Golczak, M., Jastrzebska, B., Harris, T., Ballesteros, J. A., and Palczewski, K. (2006) Crystal structure of a photoactivated deprotonated intermediate of rhodopsin. *Proc. Natl. Acad. Sci. U.S.A. 103*, 16123–16128.
49. Hubbell, W. L., Altenbach, C., and Khorana, H. G. (2003) Rhodopsin structure, dynamics and activation. *Adv. Protein Chem. 63*, 243–290.

50. Pogozheva, I. D., Przydzial, M. J., and Mosberg, H. I. (2005) Homology modeling of opioid receptor-ligand complexes using experimental constraints. *AAPS J. 7*, E434–E448.
51. Pogozheva, I. D., Chai, B. X., Lomize, A. L., Fong, T. M., Weinberg, D. H., Nargund, R. P., Mulholland, M. W., Gantz, I., and Mosberg, H. I. (2005) Interactions of human melanocortin 4 receptor with nonpeptide and peptide agonists. *Biochemistry 44*, 11329–11341.
52. Clement, M., Martin, S. S., Beaulieu, M. E., Chamberland, C., Lavigne, P., Leduc, R., Guillemette, G., and Escher, E. (2005) Determining the environment of the ligand binding pocket of the human angiotensin II type I (hAT1) receptor using the methionine proximity assay. *J. Biol. Chem. 280*, 27121–27129.
53. Oliveira, L., Costa-Neto, C. M., Nakaie, C. R., Schreier, S., Shimuta, S. I., and Paiva, A. C. (2007) The angiotensin II AT1 receptor structure-activity correlations in the light of rhodopsin structure. *Physiol. Rev. 87*, 565–592.
54. Sköld, C., Nikiforovich, G. V., and Karlen, A. (2008) Model of the angiotensin II type-2 receptor for exploring the binding mode of angiotensin II and pseudopeptide analogues, *J. Mol. Graphics Modell. 26*, 991–1003.
55. Nikiforovich, G. V., and Marshall, G. R. (2001) 3D model for TM region of the AT-1 receptor in complex with angiotensin II independently validated by site-directed mutagenesis data. *Biochem. Biophys. Res. Commun. 286*, 1204–1211.
56. Vabeno, J., Nikiforovich, G. V., and Marshall, G. R. (2006) Insight into the binding mode for cyclopentapeptide antagonists of the CXCR4 receptor. *Chem. Biol. Drug Des. 67*, 346–354.
57. Slusarz, M. J., Sikorska, E., Slusarz, R., and Ciarkowski, J. (2006) Molecular docking-based study of vasopressin analogues modified at positions 2 and 3 with N-methylphenylalanine: Influence on receptor-bound conformations and interactions with vasopressin and oxytocin receptors. *J. Med. Chem. 49*, 2463–2469.
58. Slusarz, M. J., Slusarz, R., and Ciarkowski, J. (2006) Investigation of mechanism of desmopressin binding in vasopressin V2 receptor versus vasopressin V1a and oxytocin receptors: Molecular dynamics simulation of the agonist-bound state in the membrane-aqueous system. *Biopolymers 81*, 321–338.
59. Crump, M. P., Gong, J. H., Loetscher, P., Rajarathnam, K., Amara, A., Arenzana-Seisdedos, F., Virelizier, J. L., Baggiolini, M., Sykes, B. D., and Clark-Lewis, I. (1997) Solution structure and basis for functional activity of stromal cell-derived factor-1; dissociation of CXCR4 activation from binding and inhibition of HIV-1. *EMBO J. 16*, 6996–7007.

BI702321A